




Article

Mg,Sr-Cosubstituted Hydroxyapatite with Improved Structural Properties

Elena Landi ¹, Stefano Guizzardi ², Elettra Papa ¹ and Carlo Galli ^{2,*}

¹ ISTE-CNR, Institute of Science and Technology for Ceramics-National Research Council, Via Granarolo 64, 48018 Faenza, Italy; elena.land@istec.cnr.it (E.L.); elettra.papa@istec.cnr.it (E.P.)

² DiMeC, Department of Medicine and Surgery, University of Parma, Via Volturno 39, 43126 Parma, Italy; stefano.guizzardi@unipr.it

* Correspondence: carlo.galli@unipr.it; Tel.: +39-0521-906740

Abstract: Bone substitute materials require specific properties to make them suitable for implantation, such as biocompatibility and resistance to mechanical loads. Mg,Sr-cosubstituted hydroxyapatite (MgSr-HA) is a promising bone scaffold candidate because its structure is similar to the native bone matrix. However, MgSr-HA materials do not typically withstand thermal treatments over 800 °C, because Mg promotes HA degradation to less stable tricalcium phosphate, a compound that, albeit biocompatible, is not found in bone. We, therefore, designed an ion-exchange process to enrich sintered Sr-HA with Mg and obtain MgSr-HA porous constructs. These materials contained a 0.04–0.08 Mg/Ca molar ratio and a 0.12–0.13 Sr/Ca molar ratio, and had up to 20 MPa of compressive strength, suitable for use as bone fillers or scaffolds. Unlike previous synthetic Mg,Sr-substituted apatite powders, the proposed process did not degrade HA and thus preserved its similarity to bone structure. The obtained material thus combines the presence of bioactive Mg and Sr ions in the HA lattice with a 3D morphological/structural organization that can be customized in pore size and distribution, as well as in mechanical strength, thus potentially covering a wide range of clinical applications.



Citation: Landi, E.; Guizzardi, S.; Papa, E.; Galli, C. Mg,Sr-Cosubstituted Hydroxyapatite with Improved Structural Properties. *Appl. Sci.* **2021**, *11*, 4930. <https://doi.org/10.3390/app11114930>

Academic Editor: Cem Selcuk

Received: 3 May 2021

Accepted: 25 May 2021

Published: 27 May 2021

Publisher's Note: MDPI stays neutral with regard to jurisdictional claims in published maps and institutional affiliations.



Copyright: © 2021 by the authors. Licensee MDPI, Basel, Switzerland. This article is an open access article distributed under the terms and conditions of the Creative Commons Attribution (CC BY) license (<https://creativecommons.org/licenses/by/4.0/>).

Keywords: apatite synthesis; sintering; ion exchange; porous scaffold; characterization

1. Introduction

The progressive aging of the population, together with the increase in age-related diseases and bone impairment, requires the development of novel tissue substitutes with enhanced performance [1–3]. Calcium phosphate ceramics have long been acknowledged among the most promising materials because they resemble natural bone [4,5], whose inorganic phase basically corresponds to hydroxyapatite ($\text{Ca}_{10}(\text{PO}_4)_6(\text{OH})_2$).

In addition to calcium and phosphates, however, bone contains minor amounts of other elements, which affect hydroxyapatite stability, and thus its resorbability, while also exerting biological effects on cells [6]. It may be therefore important to devise bone substitutes that better mimic the natural composition of bone, to replicate the range of its biological interactions.

In particular, Mg is an important biologically active bivalent cation [7]. The concentration of Mg in bone peaks in the first stages of bone formation, and it then decreases as calcification progresses and during aging [8]. Severe Mg deficiency affects bone growth and causes osteopenia and skeletal fragility in animal models [9].

Sr is a natural bone-seeking trace element [8,10], which accumulates in the skeleton, preferably into newly formed bone [11,12], affects collagen synthesis in cell culture [9,10], and promotes osteoblastic function [13]. In vivo studies indicate that Sr, within a certain concentration range [14], increases bone formation and reduces bone resorption, thus improving bone mass and mechanical properties in both animals and humans, under normal or pathological bone conditions [11,12,15–18]. However, Sr in bone decreases with

age [19], similar to Mg, and oral administration alone is poorly effective in restoring higher Sr levels [11].

Numerous studies on Mg,Sr-cosubstituted calcium phosphates have been hitherto published [20–24]. Most of them mainly focused on the chemophysical and structural characterization of synthetic powders produced by wet synthesis [25–29]. However, though several *in vitro* and *in vivo* studies on single Mg- or Sr-substituted synthetic apatites are available [30–33], the literature on cosubstituted Mg,Sr apatites as bone substitutes is still scarce. Obtaining sintered Mg,Sr-cosubstituted HA is challenging because the thermal treatments used for sintering improve the chemophysical superficial stability and the mechanical properties of apatite but decrease Mg stability in the HA lattice. Moreover, to the authors' knowledge, Mg,Sr-cosubstituted apatite still lacks the morphological 3D organization and structural properties typical of sintered porous apatite scaffolds.

This research group has previously reported on the development of macro-granules of Mg,Sr cosubstituted HAs (MgSr-HAs) containing levels of Mg and Sr close to those observed in bones from young animals [28]. Due to its improved stability and release properties, this material displayed a better *in vitro* performance than similar materials, paving the way to biomimetic scaffolds capable of providing a prolonged direct supply of Mg and Sr ions to the surrounding bone. These granules, however, could not withstand the high temperatures required to attain effective sintering and were thus unsuitable to create scaffolds.

The aim of this work was to design and prepare bioactive porous bone substitutes that exploit the synergy of Mg and Sr while preserving the desirable structural properties of a porous 3D architecture, as obtained by high-temperature consolidation. To achieve that, we enriched sintered Sr-HA scaffolds with magnesium via an ion-exchange process.

2. Materials and Methods

2.1. Synthetic MgSr-HA Macro-Granules

Synthetic, 400–600 μm MgSr-HA macro-granules were used for thermal stability tests. The material was prepared through a previously described wet granulation process [28]. Briefly, $\text{MgCl}_2 \cdot 6\text{H}_2\text{O}$ and $\text{Sr}(\text{NO}_3)_2$ solutions were added to a water suspension containing 1.28 moles of $\text{Ca}(\text{OH})_2$ at 40 °C. The initial Sr/Ca and Mg/Ca molar ratios were set at 0.20 and 0.15–0.25, respectively. A solution containing 0.77 moles of H_3PO_4 was dropped into said $\text{Ca}(\text{OH})_2$ suspension, while maintaining heating and stirring. No further chemical (e.g., ammonia) was needed to maintain the high pH conditions required for the precipitation of apatite because the synthesis process is “self-controlled at high pH.” The synthesis has a high yield, is reproducible, and allows an easy scale-up. After 24 h of rest, the precipitate was washed and centrifuged, then freeze-dried and sieved at 150 μm . Porous macro-granules of 400–600 μm with the peculiar chemical–physical, compositional, and superficial properties of the starting MgSr-HA powder were thus obtained by wet granulation. These materials will be referred to as “as-prepared MgSr-HA” (apMgSr-HA).

2.2. The 3D Porous Scaffold of MgSr-HA

Two types of porous architectures were used for the study: samples were either prepared using the replica method or by direct foaming. Porous scaffolds of Sr-HA were prepared using the replica method, as previously reported [23]. Briefly, a 15 vol% aqueous suspension of Sr-HA was prepared using 1.5 wt% of dispersant (Duramax D-3021). The suspension was then homogenized using zirconia balls for 4 h. Cellulosic sponges (Spontex, Italy) were trimmed to the desired shape (about 15 mm diameter and height), soaked into the slurry, and left to dry for 24 h in the air. Sr-HA porous samples were then sintered at 1250 °C for 2 h using flowing air to promote the organic matrix elimination during the debonding step at 600 °C for 1 h.

Porous scaffolds were also prepared by directly foaming a 60 wt% aqueous suspension of Sr-HA powder containing 1.5 wt% of Dolapix CA as dispersant and 1.4 wt% of foaming

agent (Dermocin BS Conc). After casting and drying for 48 h, scaffolds were sintered at 1250 °C for 2 h in the air.

Ion-exchange treatments were then explored: the sintered Sr-HA porous constructs were immersed in 1 and 2 M solutions of $MgCl_2 \cdot 6H_2O$ for 1 and 5 days, with a material/solution ratio of 0.05 g/mL, rinsed with deionized water, dried, and subsequently analyzed. The ion-exchanged samples were correspondingly coded SM1d1, SM1d5, SM2d1, and SM2d5.

2.3. Characterizations of the Materials

2.3.1. Thermal Stability Analysis

Thermogravimetric analysis (STA 449 Netzsch) was used to explore the thermal transformation process and the thermal stability of the macro-granules: the analysis was performed on 20 mg specimens, using a heating rate of 10 °C/min up to 1350 °C.

2.3.2. XRD Analysis

X-ray diffraction analysis (Cu $K\alpha$ radiation, Rigaku) was used to assess the presence of secondary phases besides apatite and to follow up the changes in cell parameters' values and in cell volume due to the ion exchange treatments. The a, b, and c cell parameters were, respectively, calculated as $a = b = 2 \times 3^{1/2} \times D_{(300)}$ and $c = 2D_{(002)}$, and from the corresponding interplanar distances, D values related to the (300) and (002) peaks located at 25.8° and 32.8° of 2-tetha in stoichiometric HA. The crystallographic cell volume was calculated as $V = a^2 c \times \sin 120^\circ$.

2.3.3. Macro- and Microstructural Compositional Evaluation

The morphological and microstructural characterization of the materials (scaffolds and granules) was performed by scanning electron microscopy using an environmental scanning electron microscope (E-SEM FEI Quanta 200, FEI Company, USA) and a field emission gun scanning electron microscope (FE-SEM, Carl Zeiss Sigma, Germany) with energy dispersive spectroscopy capability (EDS, INCA Energy 300, Oxford Instruments, UK). The latter instrument was used to assess the chemical composition of the material before and after ion exchange and determine the element distribution in the analyzed areas as well. The characterizations were conducted on cross sections of the structured bodies and on the powdered materials to exclude inhomogeneity between the surface and the bulk. Inductively coupled plasma–optical emission spectroscopy (ICP-OES 5100 Agilent technologies) was also used to analyze the solutions after ion exchange.

2.3.4. Mechanical Characterization

Compressive strength was measured on $4.5 \times 8.5 \times 13.0 \text{ mm}^3$ ($\pm 0.5 \text{ mm}$ /side) specimens using a testing machine (Zwick Z050, GmbH, Ulm, Germany) and a cross-head speed of 2 mm/min^{-1} .

3. Results and Discussion

3.1. Thermal Stability of As-Prepared Mg,Sr-Cosubstituted HA

We previously showed that strontium cosubstitution stabilizes synthetic Mg-substituted HA in thermally untreated, as-prepared materials (apMgSr-HA) [28].

Chemophysical and in vitro tests suggested that porous macro-granules of apMgSr-HA could be used as resorbable fillers for bone defects, because these granules could release Sr and Mg ions for a longer time than the corresponding Sr-free compositions, a potential benefit for new bone formation.

High temperatures, however, degrade the apatite phase of apMgSr-HA, because of the presence of Mg, although apMgSr-HA is actually less sensitive to heat than Sr-free Mg-substituted HA, where secondary phases may form already around 400 °C [34,35].

TGA (Figure 1A) and XRD (Figure 1B–D) analyses of apMgSr-HA revealed that increasing the Mg/Ca ratio in the adopted synthesis from 0.15 to 0.25 enhanced the thermal

instability of the material. In particular, TGA and the related DTG curves showed a bigger and earlier weight loss for the apMgSr-HA powder derived from Mg/Ca reactant ratio of 0.25, compared to 0.15.

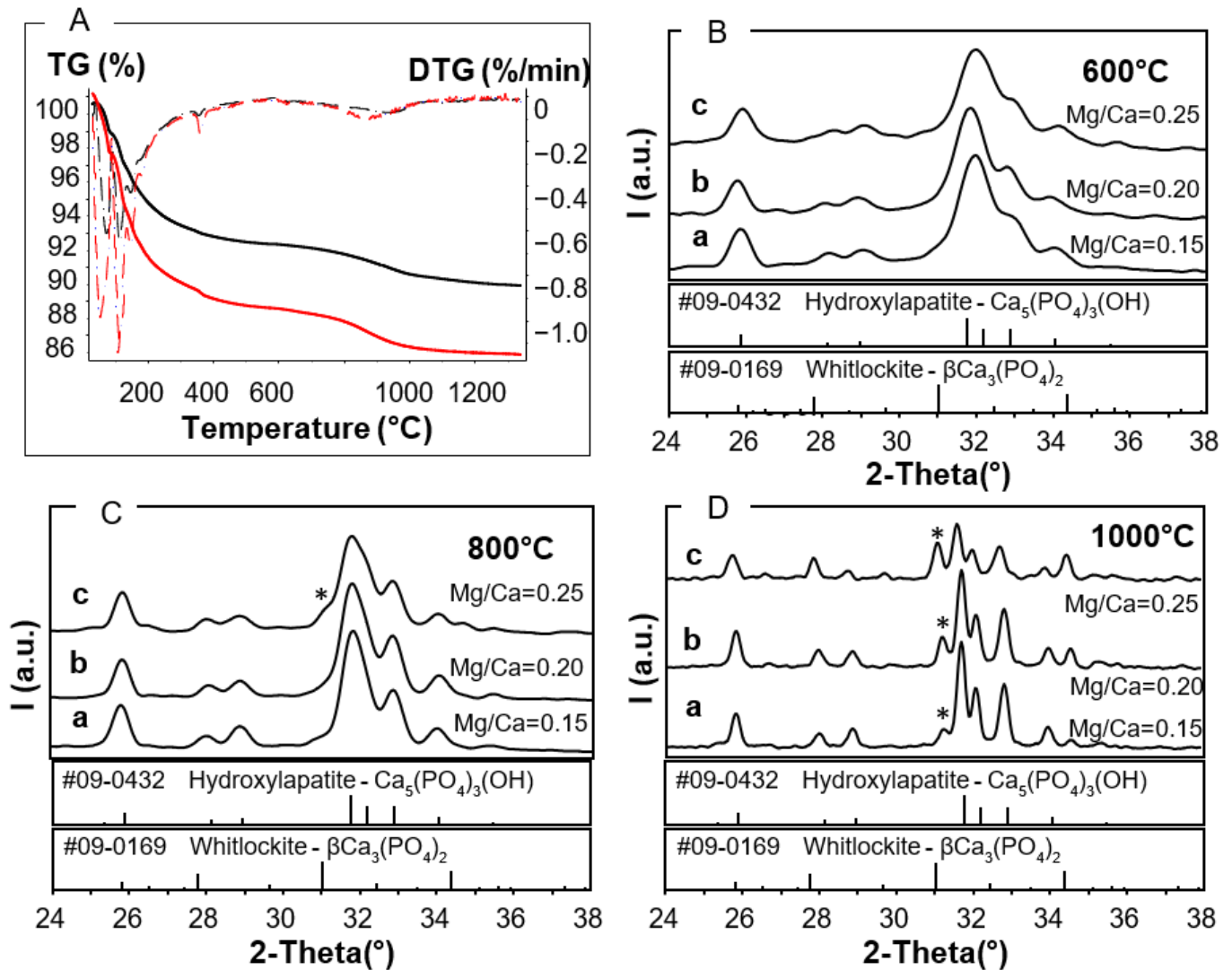


Figure 1. (A) TG (continue line) and DTG (point and line) curves of the synthetic powders prepared with synthesis molar ratios Sr/Ca = 0.20 and Mg/Ca = 0.15 (black curve) and 0.25 (red curve); (B–D) XRD spectra of the synthetic MgSr-HA granulate prepared with synthesis molar ratios Sr/Ca = 0.20 and Mg/Ca = 0.15 (a), 0.20 (b) and 0.25 (c) after thermal treatment at 600 °C (B), 800 °C (C), 1000 °C (D). The references to HA ICDD card n.09–0432 and β -TCP ICDD card n.09–0169 are indicated; * shows the signal of the main peak of β -TCP.

XRD spectra showed no secondary phases in the synthetic apMgSr-HA after heating at 600 °C, regardless of Mg concentration (Figure 1B). Secondary phases were also not observed in synthetic apMgSr-HA materials prepared with a Mg/Ca synthesis ratio of 0.15 and 0.20, after heating at 800 °C (Figure 1C), while 10–20 vol% of β -TCP was estimated to form after calcination at 1000 °C (Figure 1D). The apatite cell parameter values increased with the treatment temperature, and this trend was associated with Mg depletion.

When the starting Mg/Ca ratio was increased to 0.25, 10–15 vol% of β -TCP formed at just 800 °C (Figure 1C). The secondary phase increased up to 40–45 vol% when the material was fired at 1000 °C (Figure 1D). This higher apatite instability obtained by increasing the Mg/Ca ratio of the adopted synthesis from 0.15 to 0.25 is associated with the increase in Mg content in the powder from 1.5 wt% to 3.0 wt%. These values correspond to Mg/Ca ratios of

about 6 mol% and 12 mol%, respectively, which suggests a limited yield for ion substitution. Noteworthy, 12 mol% is beyond the maximum possible limit of substitution, which is about 9 mol%; as a consequence, the Mg in excess did not enter the HA crystallographic cell but was confined to the amorphous surface layer [28].

It could be speculated that these MgSr-HA macro-granules could be clinically used as fillers in bone defects, e.g., after surgery or trauma, and additional thermal treatments (<1000 °C) could be applied to decrease the ion release rate of the material and thus prolong its release because firing reduces material reactivity. However, the lack of morphological and structural 3D organization in a granulate biodevice may limit its use, especially when clinical conditions require a bioactive 3D porous scaffold, with suitable biomechanical features. To compound the problem further, such mechanical properties could be indeed achieved by high-temperature sintering (1250 °C), but this would degrade cosubstituted apSr,Mg-HA into secondary phases.

Therefore, an alternative strategy had to be devised to obtain sintered porous architectures made of Mg,Sr cosubstituted HA with adequate structural properties.

3.2. Ion Exchange of Mg in Sr-HA Samples: "Subsequent Mg Substitution"

3.2.1. Development of the Process

Ion exchange was previously found to be ineffective on stoichiometric sintered HA due to its low reactivity. Although ion exchange physiologically allows the incorporation of orally administered Sr into bone [12], previous attempts to replace Ca with Sr ions in HA were scarcely successful even with samples made of as-prepared, thermally untreated, and thus highly reactive, synthetic nanoapatites [36].

The exchange of Mg ions for Ca in the HA lattice of sintered samples is extremely challenging as well because Mg is not prone to enter the HA lattice even during the wet synthesis of Mg-HA powder. Evidence of ion exchange of Mg or Sr with Ca in HA has been actually reported in the literature but mostly in the hydrated surface layer of the powder nanocrystals [25].

To bypass this problem, we exploited the lattice defectiveness of sintered Sr-HA, and in particular, the HA cell expansion induced by Sr ions (which are bigger than Ca ions) to promote Mg exchange since Mg is smaller than both Ca and Sr.

3.2.2. Effectiveness of the Process

To test ion exchange, porous sintered Sr-HA scaffolds produced by either sponge impregnation (a, b, c) or by direct foaming (d, e, f) were used (Figure 2). Both scaffold types presented ultra-macropores up to millimetric scale (Figure 2a,d), which were highly interconnected through windows on the pore walls of size from hundreds to tens of microns down to micron (Figure 2b,c,e,f).

These architectures are known to perform well both *in vitro* and *in vivo* because they allow for physiological fluid permeation and cell colonization [37–39].

The porous samples of Sr-HA sintered at 1250 °C showed no secondary phases besides apatite before and after Mg ion exchange (Figure 3a,b). The elements detected by EDS (Figure 4a,b); therefore, all belonged to the apatite lattice in both cases.

The effectiveness of Mg ion exchange in Sr-HA can be explained on the basis of the opposite size of Mg and Sr ions, as compared with Ca ion size [27]: the bigger size of Sr²⁺ (1.12 Å) compensates for the smaller size of Mg²⁺ (0.89 Å), as compared to Ca²⁺ (0.99 Å), and thus, it stabilizes the cosubstituted MgSr-HA lattice.

However, the presence of two Ca sites in the HA lattice makes it difficult to evaluate the extent of single substitutions on the basis of the crystallographic cell modification, which is, however, useful to gauge the overall influence of coexisting substituting ions.

It has been reported that Mg substitutions decrease the a and c parameter values of the HA lattice, while Sr substitutions increase a and c parameter values [27,28,37,40].

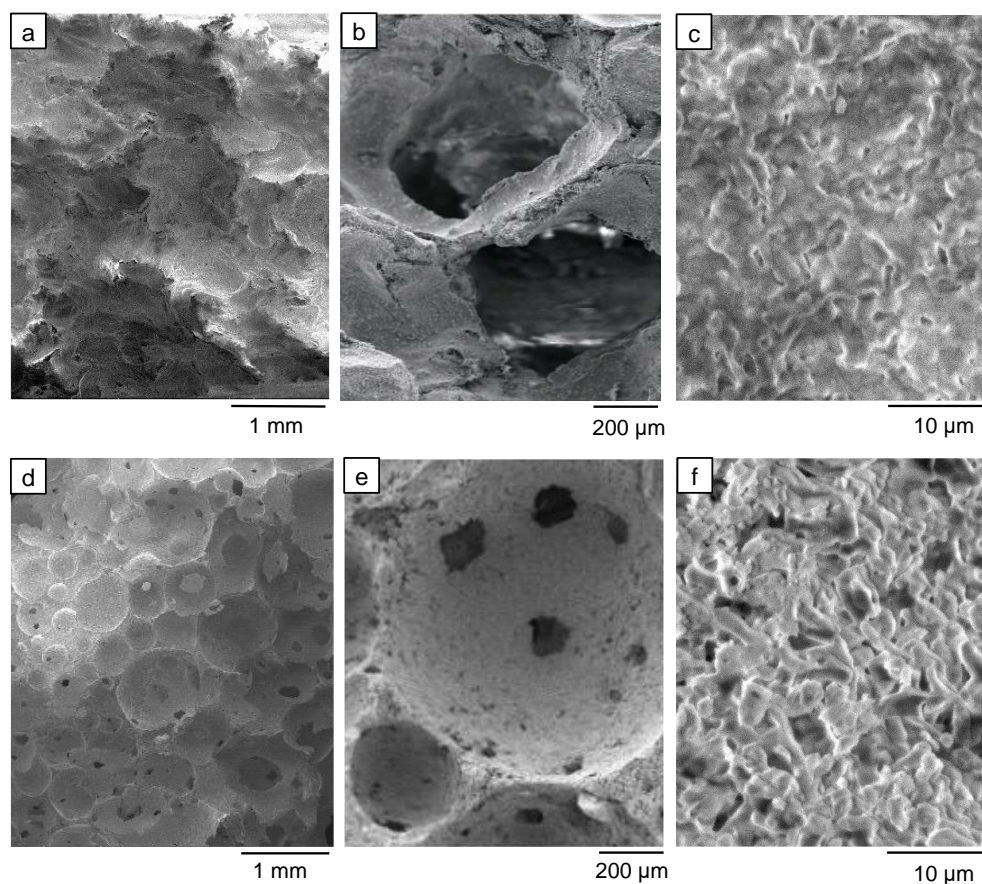


Figure 2. SEM images of the porous sintered scaffolds prepared by sponge impregnation method (a–c) and direct foaming (d–f) showing the multiscale pores affecting the constructs.

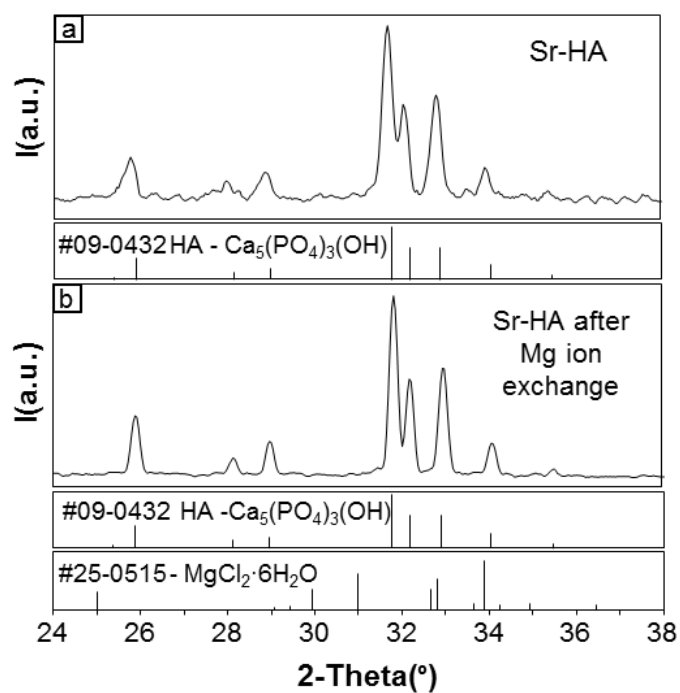


Figure 3. XRD spectra of the sintered porous Sr-HA before (a) and after the Mg ion exchange (b).

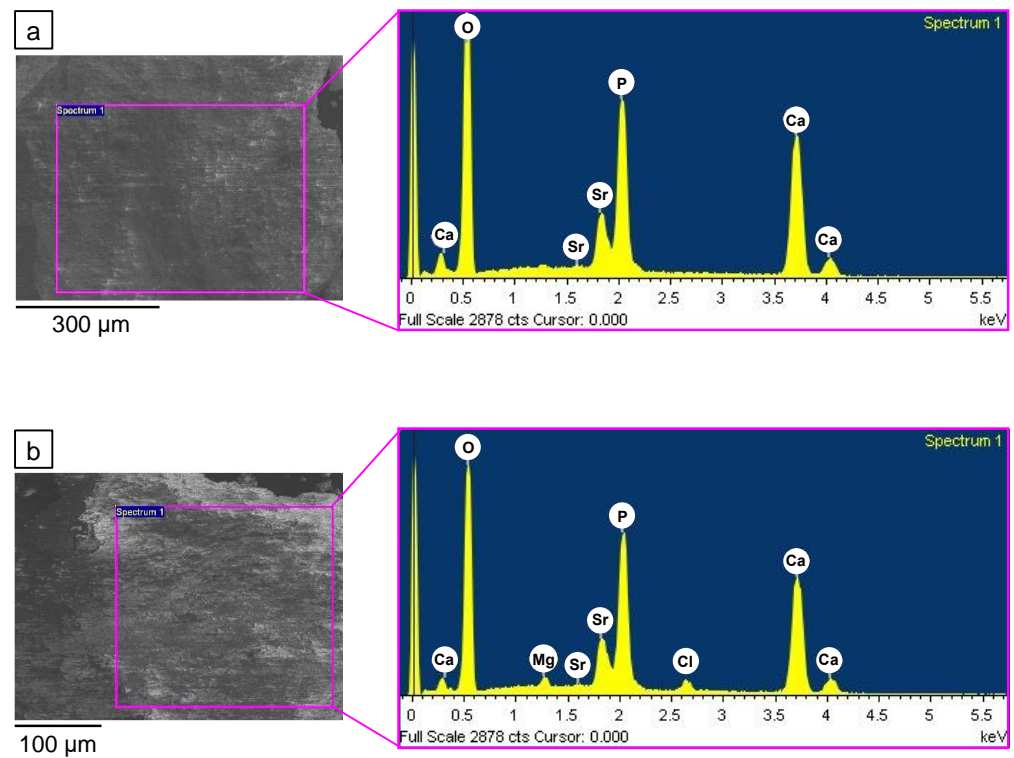


Figure 4. SEM/EDS analysis of Sr-HA scaffold material before (a) and after the ionic exchange with Mg (b). The appearance of Mg and Cl signals is evident in (b).

Although cell parameters, when taken singularly, may not be accurate, we observed a reproducible trend of volume reduction for the crystallographic cells of our scaffolds, indicating the exchange of some lattice cations with Mg ions (Table 1). A higher decrease in cell volume was observed with solutions containing higher Mg concentrations or with longer immersion. Time is a critical factor since similar crystallographic cell volumes can be obtained using different Mg concentrations, once the immersion duration is set.

Table 1. Lattice parameters and cell volume of the material before and after the ionic exchange tests.

	a (Å)	c (Å)	V (Å ³)
SrHA	9.462	6.913	536.0
SM1d1	9.418	6.880	528.4
SM1d5	9.342	6.827	516.0
SM2d1	9.407	6.879	527.2
SM2d5	9.352	6.819	516.5

The EDS analysis of numerous cross sections of the scaffold revealed a homogeneous composition and demonstrated that the Mg ion exchange process involved the whole sample and was not limited to its surface or localized areas. Figure 5 shows an example of the mapping of each element detected by EDS in the examined area (green colored in the upper image). The density of points reflects the relative amounts of the detected elements.

Noteworthy, Cl also may have been incorporated into the HA lattice since EDS (Figure 5) detected Cl quite homogeneously distributed in the sample, and no evidence of Mg chloride was observed by XRD analysis (Figure 3b). The changes in cell parameters due to Mg entrance in the HA lattice could therefore be partially hidden by the incorporation of Cl ions, which expanded the cell volume: a significant increase of a and c axis parameters was observed in Cl-apatites, as compared to HA, due to the presence of bigger Cl ions (1.81Å) substituting for OH groups (1.68Å) [41]. Other studies reported that a and c, respectively, increased or decreased together with the amount of chloride substituting

for hydroxide [42,43]. Chloride substitution, however, does not represent a problem for biomaterial applications, because Cl is physiologically present in biological systems, and it actually enhances the osteoconductivity of synthetic hydroxyapatite [43].

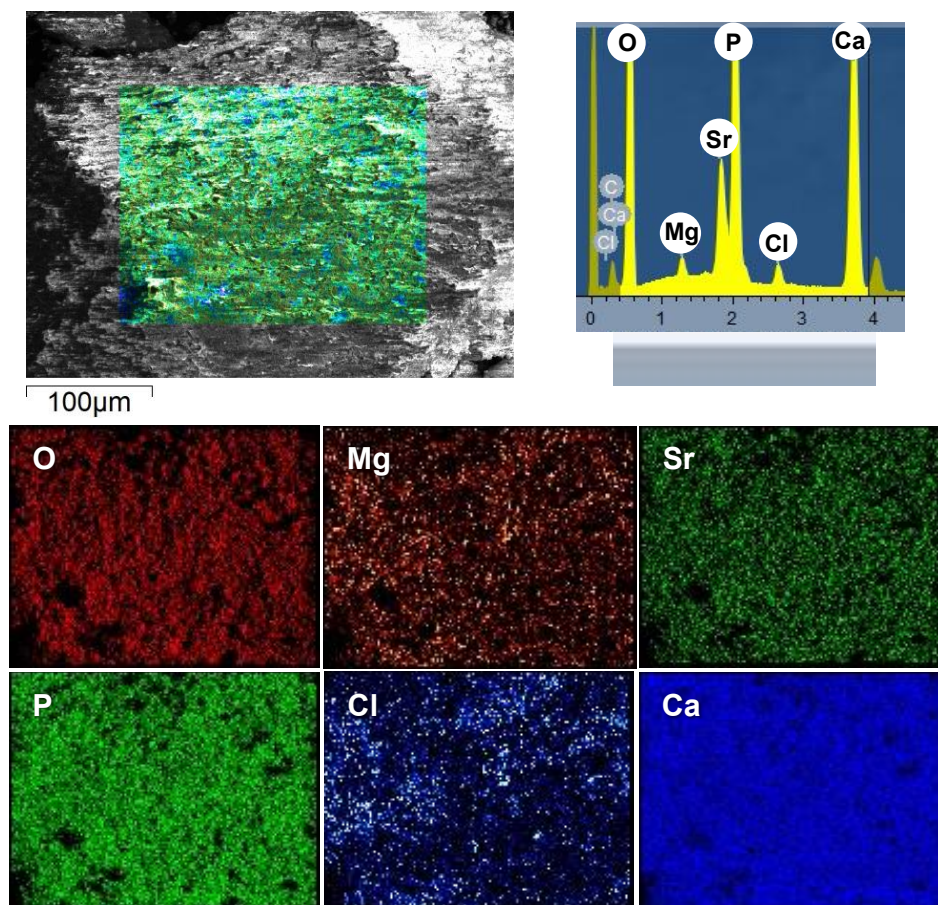


Figure 5. Maps of elements detected by SEM-EDS analysis in scaffold material after the ionic exchange with Mg. The detected elements are all uniformly distributed in the analyzed area, with points' density qualitatively reflecting their relative contents.

The XRD results were supported by EDS analysis on Sr-HA before and after Mg ion exchange. This analysis confirmed the trends in the elemental contents and molar ratios (Table 2) and highlighted that the ion exchange was already effective with 1M Mg for 1 day.

Table 2. Element contents (mean values of three measurements) and molar ratios of the sintered porous Sr-HA samples after performing the Mg ion exchange treatment using Mg solutions 1M and 2M for 1 and 5 days each.

	Ca (mol%)	P (mol%)	Mg (mol%)	Sr (mol%)	Ca/P	(cat)/P	Mg/Ca	Sr/Ca	Mg/Sr
SrHA	21.87	14.45	-	2.84	1.51	1.71	-	0.130	-
SM1d1	21.83	13.80	0.74	2.64	1.58	1.83	0.034	0.121	0.280
SM1d5	21.03	13.90	1.00	2.69	1.51	1.78	0.048	0.128	0.372
SM2d1	22.00	13.52	0.89	2.59	1.63	1.88	0.040	0.118	0.344
SM2d5	20.46	13.53	1.79	2.57	1.51	1.83	0.087	0.126	0.696

In addition, the data suggest that a preferential substitution of Sr ions is likely to have occurred first, followed by Ca ions exchange at a later stage, when exposure was extended to 5 days.

ICP-OES analysis confirmed that the ion exchange solutions were enriched in Sr and Ca and depleted in Mg but, due to high initial Mg concentrations, the data are strongly affected by dilution and/or instrumental errors, which limited the reproducibility and reliability of the obtained values. The selected conditions, however, allowed the synthetic apatite lattice to retain higher Sr concentrations than those in bone. This could be clinically beneficial since it can be envisaged that Sr ions can be released from the scaffold into the surgical receiving site and thus exert a localized therapeutic activity, possibly reducing the need for oral administration.

As for Mg, substitutions were obtained close to and beyond the maximum biological levels in hard tissues. In particular, the Mg weight content in the material after immersion in 1 M-Mg solution for 1 day was around 1.1 wt%, i.e., close to its maximum biological value.

More severe ion exchange conditions (2 M for 5 days) seemed to strongly alter the material. The Mg/Ca ratio reached about 9%, which means that the maximum possible ion exchange with Mg for Ca in the lattice was obtained and the amount of Mg exceeding that value was likely localized in the hydrated surface layer of the material [28].

The crystallographic cell volume of the material was actually quite similar among the samples after 5 days of ion exchange, regardless of Mg concentrations. However, since the stronger conditions of ion-exchange treatment were not necessary to the purpose of our study, they were disregarded for further investigations.

Both the Sr-HA architectures (sponge replica and foams) were successfully converted into MgSr-HA by ion exchange. Mg incorporation in the cationic crystallographic sites was, therefore, possible and could be adjusted by ion exchange on porous sintered Sr-HA, independently of the process used for material shaping. This feature is particularly appealing if developments in scaffold production technology, including rapid prototyping [4], are considered.

3.2.3. Evaluation of the Mechanical Properties of MgSr-HA

The process performance strictly depends on the chemical–physical properties of the powder, including its stoichiometry, because these, in turn, affect slurry concentration and stability. Low solid contents yield weak architectures, whereas high solid contents make the viscosity of the slurry unsuitable to obtain 3D porous bone substitutes [36,44].

For a given synthetic Sr-HA powder, the microstructure and the mechanical properties of the resulting porous scaffolds are strictly dependent on the forming/shaping process used. A decrease in total porosity of sponge-derived sintered Sr-HA scaffolds from 60 vol% to 45 vol% increased their compressive strength from 2 to 5 MPa [36]. These values, regardless, fall within the wide range of values reported for human bone (femur: 4–11 MPa and proximal tibia 2–8 MPa [45]).

Porous samples produced by direct foaming generally present improved compressive strength, compared to those prepared by sponge impregnation: tenfold higher values were even found for HA samples with 70 vol% of porosity (5.7 vs. 0.5 MPa), whose performance was positively tested in sheep mandibular sites [26]. Higher compressive strength for foamed samples (about 23.3 ± 2.5 MPa), compared to the sponge-derived ones (about 4.5 MPa), was again obtained with sintered Sr-HA with porosity of 45 vol%.

In addition, a preliminary test revealed that the ion-exchange-based conversion into MgSr-HA left the average compressive strength of the scaffolds (22.4 MPa) likely unaltered. Figure 6 shows two representative curves of Sr-HA foams before and after Mg ion exchange that reflect the typical behavior of porous apatite samples, where the jagged curve is indicative of the progressive rupture of the ceramic struts constituting the porous architecture.

Keeping the compressive strength value quite unmodified after ion exchange represents an additional benefit of the process because a whole range of Sr-HA products (e.g., macro-granular fillers and scaffolds with different architectures) can be generated from the same Sr-HA powder, with the possibility to convert them into MgSr-HA by just including an additional ion-exchange step.

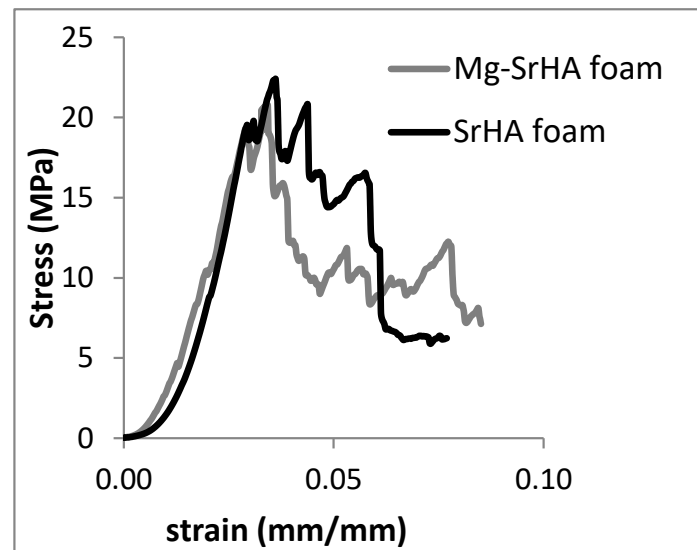


Figure 6. Compressive stress–strain curves of Sr-HA foams (45%vol of porosity) before and after Mg ion exchange, showing the proposed process is not substantially affecting the mechanical property.

4. Conclusions

MgSr-HAs have the potential to exert beneficial biological effects by releasing Mg ions in situ. Although MgSr-HA can be thermally consolidated, the maximum firing temperature of Mg-containing HAs is lower than what is used with apatite scaffolds to avoid the formation of secondary phases, and this limits their mechanical properties, and thus, their use.

Mg ion exchange on high temperature-sintered Sr-HA was exploited to prepare MgSr-HA porous scaffolds that mimicked the architecture of cancellous bone and with improved mechanical properties. This process can be applied on sintered Sr-HA materials irrespective of their 3D architecture and, based on our data, without significantly altering their compressive strength.

These improved structural properties are coupled with a chemical composition that, due to Mg and Sr incorporations, has the potential to stimulate bone metabolism and formation.

The present study, therefore, constitutes a proof of concept for viable MgSr-HA bone substitutes with characteristics that better meet clinical requirements in orthopedics and dentistry. Future studies will investigate the cellular effects of this material for further characterization of its biological properties.

Author Contributions: Conceptualization, E.L. and E.P.; methodology, E.L.; validation, E.L., S.G., and C.G.; formal analysis, E.P.; investigation, E.L. and E.P.; resources, S.G.; data curation, E.L.; writing—original draft preparation, E.L.; writing—review and editing, C.G.; visualization, C.G.; supervision, S.G. All authors have read and agreed to the published version of the manuscript.

Funding: This research received no external funding.

Institutional Review Board Statement: Not applicable.

Informed Consent Statement: Not applicable.

Data Availability Statement: The data presented in this study are available on request from the corresponding author.

Acknowledgments: This paper is published in memory of Giancarlo Celotti, senior researcher at ISTE, crystallographer of great experience, who greatly contributed to this work.

Conflicts of Interest: The authors declare no conflict of interest.

References

1. Ding, M. Age variations in the properties of human tibial trabecular bone and cartilage. *Acta Orthop. Scand. Suppl.* **2000**, *292*, 1–45. [[CrossRef](#)]
2. Chan, G.K.; Duque, G. Age-Related Bone Loss: Old Bone, New Facts. *Gerontology* **2002**, *48*, 62–71. [[CrossRef](#)]
3. Iaquinta, M.; Mazzoni, E.; Manfrini, M.; D'Agostino, A.; Trevisiol, L.; Nocini, R.; Trombelli, L.; Barbanti-Brodano, G.; Martini, F.; Tognon, M. Innovative Biomaterials for Bone Regrowth. *Int. J. Mol. Sci.* **2019**, *20*, 618. [[CrossRef](#)]
4. Habraken, W.; Habibovic, P.; Epple, M.; Bohner, M. Calcium phosphates in biomedical applications: Materials for the future? *Biochem. Pharmacol.* **2016**, *19*, 69–87. [[CrossRef](#)]
5. Fernandez de Grado, G.; Keller, L.; Idoux-Gillet, Y.; Wagner, Q.; Musset, A.-M.; Benkirane-Jessel, N.; Bornert, F.; Offner, D. Bone substitutes: A review of their characteristics, clinical use, and perspectives for large bone defects management. *J. Tissue Eng.* **2018**, *9*, 204173141877681. [[CrossRef](#)] [[PubMed](#)]
6. Ciosek, Z.; Kot, K.; Kosik-Bogacka, D.; Łanocha-Arendarczyk, N.; Rotter, I. The Effects of Calcium, Magnesium, Phosphorus, Fluoride, and Lead on Bone Tissue. *Biomolecules* **2021**, *11*, 506. [[CrossRef](#)]
7. Rondanelli, M.; Faliva, M.A.; Tartara, A.; Gasparri, C.; Perna, S.; Infantino, V.; Riva, A.; Petrangolini, G.; Peroni, G. An update on magnesium and bone health. *BioMetals* **2021**. [[CrossRef](#)] [[PubMed](#)]
8. Bigi, A.; Foresti, E.; Gregorini, R.; Ripamonti, A.; Roveri, N.; Shah, J.S. The role of magnesium on the structure of biological apatites. *Calcif. Tissue Int.* **1992**, *50*, 439–444. [[CrossRef](#)] [[PubMed](#)]
9. Rude, R.K.; Singer, F.R.; Gruber, H.E. Skeletal and hormonal effects of magnesium deficiency. *J. Am. Coll. Nutr.* **2009**, *28*, 131–141. [[CrossRef](#)] [[PubMed](#)]
10. Pors Nielsen, S. The biological role of strontium. *Bone* **2004**, *35*, 583–588. [[CrossRef](#)]
11. Dahl, S.G.; Allain, P.; Marie, P.J.; Mauras, Y.; Boivin, G.; Ammann, P.; Tsouderos, Y.; Delmas, P.D.; Christiansen, C. Incorporation and distribution of strontium in bone. *Bone* **2001**, *28*, 446–453. [[CrossRef](#)]
12. Marie, P.J.; Ammann, P.; Boivin, G.; Rey, C. Mechanisms of action and therapeutic potential of strontium in bone. *Calcif. Tissue Int.* **2001**, *69*, 121–129. [[CrossRef](#)]
13. Singh, S.S.; Roy, A.; Lee, B.; Parekh, S.; Kumta, P.N. Murine osteoblastic and osteoclastic differentiation on strontium releasing hydroxyapatite forming cements. *Mater. Sci. Eng. C* **2016**, *63*, 429–438. [[CrossRef](#)]
14. Grynepas, M.D.; Hamilton, E.; Cheung, R.; Tsouderos, Y.; Deloffre, P.; Hott, M.; Marie, P.J. Strontium increases vertebral bone volume in rats at a low dose that does not induce detectable mineralization defect. *Bone* **1996**, *18*, 253–259. [[CrossRef](#)]
15. Cattani-Lorente, M.; Rizzoli, R.; Ammann, P. In vitro bone exposure to strontium improves bone material level properties. *Acta Biomater.* **2013**, *9*, 7005–7013. [[CrossRef](#)] [[PubMed](#)]
16. Boanini, E.; Torricelli, P.; Fini, M.; Bigi, A. Osteopenic bone cell response to strontium-substituted hydroxyapatite. *J. Mater. Sci. Mater. Med.* **2011**, *22*, 2079–2088. [[CrossRef](#)] [[PubMed](#)]
17. Lavet, C.; Mabileau, G.; Chappard, D.; Rizzoli, R.; Ammann, P. Strontium ranelate stimulates trabecular bone formation in a rat tibial bone defect healing process. *Osteoporos. Int.* **2017**, 1–13. [[CrossRef](#)]
18. Querido, W.; Rossi, A.L.; Farina, M. The effects of strontium on bone mineral: A review on current knowledge and microanalytical approaches. *Micron* **2016**, *80*, 122–134. [[CrossRef](#)]
19. Cazalhou, S.; Combes, C.; Rey, C. Biomimetic Approach for Strontium-Containing Ca-P Bioceramics with Enhanced Biological Activity. *Key Eng. Mater.* **2000**, 192–195, 147–150. [[CrossRef](#)]
20. Meininger, S.; Moseke, C.; Spatz, K.; März, E.; Blum, C.; Ewald, A.; Vorndran, E. Effect of strontium substitution on the material properties and osteogenic potential of 3D powder printed magnesium phosphate scaffolds. *Mater. Sci. Eng. C* **2019**, *98*, 1145–1158. [[CrossRef](#)]
21. Gu, Y.; Zhang, J.; Zhang, X.; Liang, G.; Xu, T.; Niu, W. Three-dimensional Printed Mg-Doped β -TCP Bone Tissue Engineering Scaffolds: Effects of Magnesium Ion Concentration on Osteogenesis and Angiogenesis In Vitro. *Tissue Eng. Regen. Med.* **2019**, *16*, 415–429. [[CrossRef](#)] [[PubMed](#)]
22. Scalera, F.; Palazzo, B.; Barca, A.; Gervaso, F. Sintering of magnesium-strontium doped hydroxyapatite nanocrystals: Towards the production of 3D biomimetic bone scaffolds. *J. Biomed. Mater. Res. Part A* **2020**, *108*, 633–644. [[CrossRef](#)] [[PubMed](#)]
23. Yedekçi, B.; Tezcaner, A.; Alshemary, A.Z.; Yılmaz, B.; Demir, T.; Evis, Z. Synthesis and sintering of B, Sr, Mg multi-doped hydroxyapatites: Structural, mechanical and biological characterization. *J. Mech. Behav. Biomed. Mater.* **2021**, *115*, 104230. [[CrossRef](#)] [[PubMed](#)]
24. Arkin, V.H.; Narendrakumar, U.; Madhyastha, H.; Manjubala, I. Characterization and In Vitro Evaluations of Injectable Calcium Phosphate Cement Doped with Magnesium and Strontium. *ACS Omega* **2021**, *6*, 2477–2486. [[CrossRef](#)]
25. Drouet, C.; Carayon, M.-T.; Combes, C.; Rey, C. Surface enrichment of biomimetic apatites with biologically-active ions Mg^{2+} and Sr^{2+} : A preamble to the activation of bone repair materials. *Mater. Sci. Eng. C* **2008**, *28*, 1544–1550. [[CrossRef](#)]
26. Aina, V.; Lusvardi, G.; Annaz, B.; Gibson, I.R.; Imrie, F.E.; Malavasi, G.; Menabue, L.; Cerrato, G.; Martra, G. Magnesium- and strontium-co-substituted hydroxyapatite: The effects of doped-ions on the structure and chemico-physical properties. *J. Mater. Sci. Mater. Med.* **2012**, *23*, 2867–2879. [[CrossRef](#)]
27. Kannan, S.; Goetz-Neunhoeffler, F.; Neubauer, J.; Pina, S.; Torres, P.M.C.; Ferreira, J.M.F. Synthesis and structural characterization of strontium- and magnesium-co-substituted β -tricalcium phosphate. *Acta Biomater.* **2010**, *6*, 571–576. [[CrossRef](#)]

28. Landi, E.; Uggeri, J.; Medri, V.; Guizzardi, S. Sr, Mg cosubstituted HA porous macro-granules: Potentialities as resorbable bone filler with antiosteoporotic functions. *J. Biomed. Mater. Res. Part A* **2013**, *101A*, 2481–2490. [[CrossRef](#)]
29. Geng, Z.; Wang, R.; Li, Z.; Cui, Z.; Zhu, S.; Liang, Y.; Liu, Y.; Huijing, B.; Li, X.; Huo, Q.; et al. Synthesis, characterization and biological evaluation of strontium/magnesium-co-substituted hydroxyapatite. *J. Biomater. Appl.* **2016**, *31*, 140–151. [[CrossRef](#)]
30. Ballouze, R.; Marahat, M.H.; Mohamad, S.; Saidin, N.A.; Kasim, S.R.; Ooi, J.P. Biocompatible magnesium-doped biphasic calcium phosphate for bone regeneration. *J. Biomed. Mater. Res. Part B Appl. Biomater.* **2021**. [[CrossRef](#)]
31. Santos, G.G.; Nunes, V.L.C.; Marinho, S.M.O.C.; Santos, S.R.A.; Rossi, A.M.; Miguel, F.B. Biological behavior of magnesium-substituted hydroxyapatite during bone repair. *Brazilian J. Biol.* **2021**, *81*, 53–61. [[CrossRef](#)] [[PubMed](#)]
32. Swain, S.; Bowen, C.; Rautray, T. Dual response of osteoblast activity and antibacterial properties of polarized strontium substituted hydroxyapatite—Barium strontium titanate composites with controlled strontium substitution. *J. Biomed. Mater. Res. Part A* **2021**, *37*, 195. [[CrossRef](#)] [[PubMed](#)]
33. Zhao, R.; Chen, S.; Zhao, W.; Yang, L.; Yuan, B.; Ioan, V.S.; Iulian, A.V.; Yang, X.; Zhu, X.; Zhang, X. A bioceramic scaffold composed of strontium-doped three-dimensional hydroxyapatite whiskers for enhanced bone regeneration in osteoporotic defects. *Theranostics* **2020**, *10*, 1572–1589. [[CrossRef](#)]
34. Fadeev, I.V.; Shvorneva, L.I.; Barinov, S.M.; Orlovskii, V.P. Synthesis and Structure of Magnesium-Substituted Hydroxyapatite. *Inorg. Mater.* **2003**, *39*, 947–950. [[CrossRef](#)]
35. Bigi, A.; Marchetti, F.; Ripamonti, A.; Roveri, N.; Foresti, E. Magnesium and strontium interaction with carbonate-containing hydroxyapatite in aqueous medium. *J. Inorg. Biochem.* **1981**, *15*, 317–327. [[CrossRef](#)]
36. Landi, E.; Tampieri, A.; Celotti, G.; Sprio, S.; Sandri, M.; Logroscino, G. Sr-substituted hydroxyapatites for osteoporotic bone replacement. *Acta Biomater.* **2007**, *3*, 961–969. [[CrossRef](#)] [[PubMed](#)]
37. Landi, E.; Celotti, G.; Logroscino, G.; Tampieri, A. Carbonated hydroxyapatite as bone substitute. *J. Eur. Ceram. Soc.* **2003**, *23*, 2931–2937. [[CrossRef](#)]
38. Ciocca, L.; Donati, D.; Fantini, M.; Landi, E.; Piattelli, A.; Iezzi, G.; Tampieri, A.; Spadari, A.; Romagnoli, N.; Scotti, R. CAD–CAM-generated hydroxyapatite scaffold to replace the mandibular condyle in sheep: Preliminary results. *J. Biomater. Appl.* **2013**, *28*, 207–218. [[CrossRef](#)]
39. Zhu, Y.; Goh, C.; Shrestha, A. Biomaterial Properties Modulating Bone Regeneration. *Macromol. Biosci.* **2021**, *21*, 2000365. [[CrossRef](#)]
40. Le Geroz, R. Calcium Phosphates in Oral Biology and Medicine. In *Monographs in Oral Science*; Myers, H., Ed.; Karger Publishers: Basel, Switzerland, 1991; pp. 82–107.
41. Cai, Y.; Zhang, S.; Ong, S.; Zeng, X.; Wang, W. Simultaneous Incorporation of Magnesium and Fluorine Ions in Hydroxyapatite Coatings on Metallic Implant for Osseointegration and Stability. In *Hydroxyapatite Coatings for Biomedical Applications*; Zhang, S., Ed.; CRC Press: Boca Raton, FL, USA, 2013; pp. 55–144.
42. Driessens, F.; Verbeek, R. Effects of chloride on the calcium rich calcium phosphates of the system $\text{Ca}(\text{OH})_2\text{-H}_3\text{PO}_4\text{-H}_2\text{O}$. In *Biomaterials*; CRC Press: Boca Raton, FL, USA, 1990.
43. Cho, J.S.; Yoo, D.S.; Chung, Y.-C.; Rhee, S.-H. Enhanced bioactivity and osteoconductivity of hydroxyapatite through chloride substitution. *J. Biomed. Mater. Res. Part A* **2014**, *102*, 455–469. [[CrossRef](#)]
44. Guicciardi, S.; Galassi, C.; Landi, E.; Tampieri, A.; Satou, K.; Pezzotti, G. Rheological characteristics of slurry controlling the microstructure and the compressive strength behavior of biomimetic hydroxyapatite. *J. Mater. Res.* **2001**, *16*, 163–170. [[CrossRef](#)]
45. Liebschner, M.A.K. Biomechanical considerations of animal models used in tissue engineering of bone. *Biomaterials* **2004**, *25*, 1697–1714. [[CrossRef](#)]